Bulletin of Glaciological Research 42 (2024) *49–60*
doi: 10.5331/bgr.24A02

[Article]

Major metallic elements (Al, Ca, and Fe) and size distribution of mineral particles in recent snow in inland Northeast Greenland

Yuki KOMURO[1,2*], Fumio NAKAZAWA[1,3], Kumiko GOTO-AZUMA[1,3], Motohiro HIRABAYASHI[1], Wataru SHIGEYAMA[3], Koji FUJITA[4], Jørgen Peder STEFFENSEN[5], Dorthe DAHL-JENSEN[5]

1 National Institute of Polar Research, 10–3 Midori-cho, Tachikawa-shi, Tokyo 190–8518, Japan
* yuuki.komuro@npofuji3776.org
2 Laboratory for Environmental Research at Mount Fuji, 2–5–5 Okubo, Shinjuku-ku, Tokyo 169–0072, Japan
3 The Graduate University for Advanced Studies, SOKENDAI, 10–3 Midori-cho, Tachikawa-shi, Tokyo 190–8518, Japan
4 Graduate School of Environmental Studies, Nagoya University, Furo-cho, Chikusa-ku, Nagoya 464–8601, Japan
5 Physics of Ice Climate and Earth, Niels Bohr Institute, University of Copenhagen, Tagensvej 16, DK-2200 Copenhagen N, Denmark

(Received April 15, 2024; Revised manuscript accepted July 5, 2024)

Abstract

Rising temperatures and melting of snow and ice since 2000 CE may result in coastal soil regions in Greenland providing more mineral particles to the Greenland ice sheet than before. To examine seasonal variations of the concentrations and source regions of mineral particles in recent snow in inland Northeast Greenland, we analyzed the total (*i.e.*, soluble and insoluble) concentrations of major metallic elements (Al, Ca, and Fe) and the size distributions of mineral particles in snow pit samples covering 2013–2017 at the East Greenland Ice Core Project site. The total concentrations of metallic elements showed clear seasonality with spring maxima, indicating that the mineral particle concentrations peaked in this season. Volcanic products from the 2014–2015 eruptions of Bárðarbunga, Iceland, had little effect on the metallic element concentrations. The increased Ca/Al ratio, Ca solubility, and fine particle fraction (≤5μm) in winter–spring indicated that the relative contributions of mineral particles originating from distant arid regions increased in those seasons. In summer–autumn, the Ca/Al ratio and Ca solubility decreased, and the coarse particle fraction (>5μm) increased, suggesting that the relative contributions from coastal soil regions in Greenland increased in those seasons.

Key words: Greenland, Snow pit, Mineral particles, Metallic element, Size distribution

1. Introduction

Mineral particles contained in the Greenland ice sheet provide information about their source regions, their transport pathways, and the past climate and environment in Greenland. To understand past climatic and environmental changes, the concentrations, fluxes, mineralogy, and strontium/neodymium isotopic ratios in Greenland ice cores have been investigated (*e.g.*, Biscaye *et al.*, 1997; Steffensen, 1997; Svensson *et al.*, 2000; Ruth *et al.*, 2002). Studies of deep ice cores from inland sites on the Greenland ice sheet found that mineral particle concentrations strongly correlated with temperature changes and were 10- to 100-fold higher in glacial periods than in interglacial periods (*e.g.*, Steffensen, 1997; Ruth *et al.*, 2002). The mineralogy and strontium/neodymium isotopic ratio analysis of the mineral particles in the inland ice cores (Greenland Ice Core Project [GRIP] and Greenland Ice Sheet Project 2) showed that Asian arid regions (*e.g.*, the Taklamakan Desert) are the most likely sources of the particles during both the Holocene and the last glacial period (Biscaye *et al.*, 1997; Svensson *et al.*, 2000). The isotopic ratio analyses of mineral particles in an ice core from an inland site (Dye-3) from the 1786–1793 period indicated Asia as their primary source and North Africa as an additional source (Lupker *et al.*, 2010). The isotopic ratio analysis of mineral particles in snow pit samples collected from the inland site (North Greenland Ice Core Project [NGRIP]) covering the 1998–2001 period suggested that the mineral particles come from the Asian regions in all seasons (Bory *et al.*, 2003a). Bory *et al.* (2003b) compared ice core data from various sites in Greenland and found that the concentrations, fluxes, mineralogy, and isotopic ratios of mineral particles at the coastal sites (Renland and Hans Tausen) differed substantially from those at the inland sites (GRIP, NGRIP, and Dye-3). Simonsen *et al.* (2019) found that mineral particles collected from Renland were dominated by those originating from the coastal soil regions in Greenland

during interglacial periods because the Greenland ice sheet retreated, exposing the coastal soils. Recent coastal ice core studies in Greenland have focused on changes in mineral particle emissions from the coastal soil regions in Greenland due to warming after 2000 CE (Amino *et al*., 2021; Nagatsuka *et al*., 2021). Amino *et al*. (2021) found a higher annual flux of mineral particles during the 2000–2014 period at the SE-Dome site in the southeastern part of the Greenland ice sheet compared with that during the 1960–2014 period. They showed that mineral particle emissions increased due to the decreased snow-covered area in Greenland resulting from warming after 2000 CE. Nagatsuka *et al*. (2021) analyzed the mineralogy and morphology of mineral particles contained in an ice core drilled from the SIGMA-D site in northwestern Greenland. They demonstrated that the mineral particle supply from the coastal soil regions in western Greenland increased during 2005–2013 and 1915–1949 due to the higher air temperature and shorter snow cover duration in the coastal regions in the two periods. Therefore, after 2000 CE, the mineral particle emissions from coastal soil regions in Greenland have likely been increasing. In particular, the mineral particle emissions are likely increasing in autumn due to the recent decrease in snow-covered area in Greenland in this season (Amino *et al*., 2021). The contribution of mineral particles from the soil regions on the Greenland coast may be increasing not only in the coastal regions, but also in the inland regions of the Greenland ice sheet (Kjær *et al*., 2022). However, in the inland regions of the Greenland ice sheet after 2000 CE, the seasonality of concentrations and source regions of mineral particles are not fully understood because there are few previous studies (Carmagnola *et al.,* 2013; Kjær *et al*., 2022).

Metallic components must be analyzed to estimate the mineral particle concentrations and fluxes on the ice sheet. Al is a major element that accounts for about 8% of the continental crust by weight, and thus it is used as a proxy for mineral particles (Wedepohl, 1995; Spolaor *et al*., 2013; Sato *et al*., 2013). In previous studies, usually only the soluble metallic components in snow and ice have been analyzed using ion chromatography (*e.g.*, Dibb *et al*., 2007; Kuramoto *et al*., 2011; Nakazawa *et al*., 2021). However, mineral particles also have insoluble components, and thus it is necessary to obtain the total (*i.e.,* soluble and insoluble) concentrations of metals for quantitative analysis of the metallic elements derived from mineral particles (*e.g.*, Sato *et al*., 2013).

The metallic composition of mineral particles in snow and ice reflects the composition of their source regions. A large amount of Ca is concentrated in arid regions as soluble calcium salts (*e.g.*, calcite and gypsum) (Formenti *et al*., 2011). Therefore, the Ca contents of mineral particles in snow and ice can be used to evaluate the supply of particles from arid regions. The Ca/Al ratio of mineral particles in snow and ice can be used as a proxy corresponds to the Ca contents. Similarly, because the calcium salts are soluble, the mineral particles from arid regions should have a higher Ca solubility, and the Ca solubility of mineral particles in snow and ice can be used to identify the particle source.

The source regions of mineral particles are also investigated by measuring the particle size distribution, which is generally measured by insoluble particle analysis with the Coulter counter method (*e.g.*, Baccolo *et al*., 2018; Simonsen *et al*., 2019). The atmospheric residence time of mineral particles depends on their diameter, and the larger the diameter, the shorter the residence time (Tegen and Lacis, 1996). Therefore, mineral particles transported from distant regions are dominated by smaller particles (Biscaye *et al*., 1997; Bory *et al*., 2003b). For example, because of the large contribution of long-range transported mineral particles, particles less than 4 μm in diameter accounted for approximately 90% of the particle mass in the central region of the Greenland ice sheet (GRIP) during the Holocene (Steffensen *et al*., 1997). In contrast, mineral particles transported from the coastal soil regions in Greenland showed large fractions of coarse particles (>5 μm) (Steffensen *et al*., 2001; Simonsen *et al*., 2019), and the coarse mineral particles were treated as originating mainly from the coastal soil regions in Greenland (Simonsen *et al*., 2019; Amino *et al*., 2021). Thus, the coarse particle fraction of total mineral particles can be used to assess the relative contribution of mineral particles originating from coastal soil regions in Greenland (Amino *et al*., 2021).

This study aims to reveal the recent temporal variations of the concentration and source regions of mineral particles with seasonal resolution in the inland region of the Greenland ice sheet. For this aim, we conducted snow pit observations at the East Greenland Ice Core Project (EGRIP) site (75.38° N, 36.00° W, 2720 m above sea level), a northeastern inland site on the ice sheet, and we measured the total concentration of metals and the size distribution of insoluble particles in the snow pit samples. Additionally, to examine the Ca solubility and the contribution of volcanic products to the concentration of metals and insoluble particles, we measured the concentrations of soluble components in the snow pit samples.

2. Methods

2.1 Sampling and measurements

The snow samples used in this study were collected from a snow pit observation at the EGRIP site on June 16, 2017 (Fig. 1). The snow pit was named Pit 4 by Komuro *et al*. (2021), who reported details of its observation and dating. The snow pit was 2.01 m in depth and covered the years 2013 to 2017. Snow samples for chemical and insoluble particle analyses were collected every 0.03 m from the surface to the bottom of the pit. The samples were collected using a pre-cleaned plastic spatula and ceramic knife and were placed in dust-free plastic bags

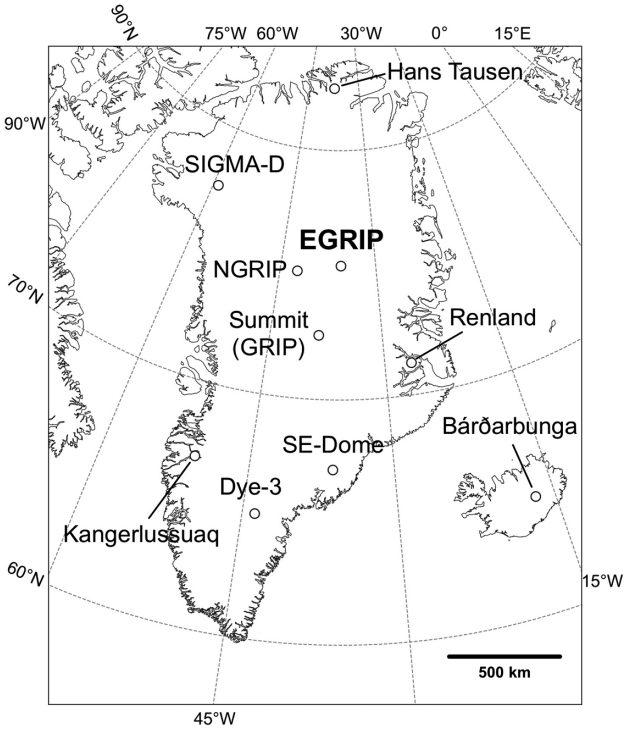

Fig. 1. Map of the study sites.

for chemical analyses and in pre-cleaned Nalgene straight-side wide-mouth jars for insoluble particle analysis. The samples were frozen and transported to the National Institute of Polar Research (NIPR).

The snow samples were melted in the Class 10,000 clean room at NIPR. The samples for insoluble particle analysis were transferred to pre-cleaned 20 mL glass bottles (Nichiden-Rika), and those for chemical analyses were transferred to pre-cleaned polypropylene bottles (surface contamination control 100 mL bottle, AS ONE). The concentrations and size distribution of insoluble particles (diameters of 0.52–12 μm) were measured with a Coulter counter (Multisizer 4, Beckman Coulter) in the Class 10,000 clean room. The error of the measured values was approximately 10 % (Nakazawa *et al.*, 2021). To calculate Ca solubility and examine the supply of volcanic products, Ca^{2+}, SO_4^{2-}, and F^- concentrations were measured from part of the samples for chemical analyses with two sets of ion chromatographs (ICS-5000 +, Thermo Fisher Scientific) in the Class 10,000 clean room. The analytical precision was better than 2 % at the 1 ng mL^{-1} level for all ions (Nakazawa *et al.*, 2021). For oxygen isotope ratios of water ($\delta^{18}O$), we used measurement data reported by Komuro *et al.* 2021. For the total concentration analysis of metallic elements, 2 mL of the samples for chemical analyses was dispensed into perfluoroalkoxy alkane (PFA) vials (Savillex), and then 0.1 mL HNO_3 (Tama Chemicals) and 0.05 mL HF (Tama Chemicals) was added to the vials in the Class 100 clean room. After the PFA vials were sealed, they were covered with polypropylene and PTFE microwave decomposition jacket assemblies (San-ai Kagaku). The particulates in the samples in the vials were decomposed by microwave radiation for 2.5 min using a 600 W microwave oven. The decomposed sample solution in the PFA vials was entirely evaporated, and then 0.5 mL HNO_3 was added to the sample residue in the vials. After evaporating the sample solution again, the sample residue in the vials was dissolved with 1 % HNO_3 in a 10 mL flask. The total concentrations of Al, Ca, Fe, and Na (Al_{total}, Ca_{total}, Fe_{total}, and Na_{total}, respectively) in the sample solution were measured by inductively coupled plasma mass spectrometry (7700 ICP-MS, Agilent Technologies). The total concentrations were not obtained for the samples from depths of 0.03–0.06 and 1.23–1.26 m because the sample volumes were not sufficient to perform the total concentration analysis.

Mineral particle concentrations in samples can be estimated from Al_{total} (Sato *et al.*, 2013). In this study, assuming that all Al_{total} is of crustal origin, the mineral particle concentration ($[C_{mineral}]$) was calculated by

$$[C_{mineral}]=[Al_{total}]/8.23\times100$$

where 8.23 is the percentage of Al abundance in the crust (Taylor, 1964). The non-sea salt fractions of Ca_{total} and SO_4^{2-} ($[nssCa_{total}]$ and $[nssSO_4^{2-}]$) were calculated by

$$[nssCa_{total}]=[Ca_{total}]-(Ca^{2+}/Na^{+})_{sea}\times[ssNa]$$

$$[nssSO_4^{2-}]=[SO_4^{2-}]-(SO_4^{2-}/Na^{+})_{sea}\times[ssNa]$$

where $(Ca^{2+}/Na^{+})_{sea}$ and $(SO_4^{2-}/Na^{+})_{sea}$ are the Ca^{2+}/Na^{+} and SO_4^{2-}/Na^{+} ratios of seawater (0.0371 and 0.254) (Broecker and Peng, 1982), respectively, and $[ssNa]$ is the sea salt-origin Na concentration. The soluble non-sea salt Ca (nssCa) concentration was calculated by

$$[nssCa_{soluble}]=[Ca_{soluble}]-(Ca/Na)_{sea}\times[ssNa]$$

and the soluble nssCa fraction was calculated by

$$F_{soluble}=[nssCa_{soluble}]/[nssCa_{total}]$$

where $[nssCa_{soluble}]$ is the soluble nssCa concentration, $F_{soluble}$ is the soluble nssCa fraction, and $[Ca_{soluble}]$ is the soluble Ca concentration measured by ion chromatography. Assuming that all Al_{total} is crustal in origin, sea salt-origin Na concentration was calculated by (Sato *et al.*, 2013)

$$[ssNa]=[Na_{total}]-(Na/Al)_{crust}\times[Al_{total}]$$

where $(Na/Al)_{crust}$ is the Na/Al ratio in the crust (0.287) (Taylor, 1964).

2.2 Back-trajectory analysis

To investigate the source regions of the mineral particles, the transport pathways of the air masses that reached EGRIP during 2013–2017 were calculated by the Hybrid Single-Particle Lagrangian Integrated Trajectory (HYSPLIT) model (Stein *et al.*, 2015) distributed by the National Oceanic and Atmospheric Administration. We used NCEP/NCAR reanalysis dataset (Kalnay *et al.*, 1996) to run the HYSPLIT model. The starting points were set

at 50, 500, 1000 and 1500 m above ground level (a.g.l.) at EGRIP (Nagatsuka *et al.*, 2021). We started the back-trajectory every 6 hours. The sum of air masses at the four altitudes was used for our analysis. The probability distribution of the air mass below 1500 m a.g.l. was calculated with a spatial resolution of 1° (Nagatsuka *et al.*, 2021). The regional contribution from the probability distribution was also calculated.

3. Results and discussion

3.1 Dating and profiles of major metallic elements, $nssSO_4^{2-}$, and F^-

The date for each layer was determined by the $\delta^{18}O$ profile (Fig. 2). The local maxima and minima of the $\delta^{18}O$ were assigned to summer and winter centers for each year, as reported by Komuro *et al.* (2021). For the seasonal analysis of pit data, we assigned seasons to not only the layers of summer and winter centers but also other layers. In this assignment, we assumed that the summer and winter centers are January 15 and July 17, respectively, for each year, and that the progression of time between the centers corresponds linearly to the change in depth between the centers. The date of the surface (depth of 0.00 m) was set to June 15, 2017, assuming that the surface snow was deposited on the day before the observation date. We did not assign the seasons for the layers below the 2013 summer center (below 1.83 m), because we could not determine the 2012/13 winter. Based on these assumptions, we determined the layers of spring (March-May), summer (June-August), autumn (September-November), and winter (December-February) (Fig. 2).

The depth profiles for the metallic elements, $nssCa_{total}/Al_{total}$ ratio (corresponding to the Ca/Al ratio and Ca content in mineral particles), soluble nssCa fraction, $nssSO_4^{2-}$, and F^- along with the $\delta^{18}O$ profile are shown in Fig. 2. The Al_{total} concentration showed clear seasonal variation, with higher concentrations in spring and lower concentrations in other seasons. The seasonal variations of Fe_{total} and $nssCa_{total}$ concentrations were similar to that of the Al_{total} concentration. The Fe_{total} and $nssCa_{total}$ concentrations were strongly correlated with the Al_{total} concentration ($r=0.95$, $p<0.001$ and $r=0.89$, $p<0.001$, respectively). The $nssCa_{total}/Al_{total}$ ratios and soluble nssCa fraction were higher in winter–spring and lower in summer–autumn. However, unseasonal increases in the soluble nssCa fraction were observed in autumn 2014. The concentrations of $nssSO_4^{2-}$ and F^- were higher in the depth range of 0.90–1.32 m (summer 2014 to summer 2015) than in the other depth ranges.

The increase in $nssSO_4^{2-}$ and F^- in the summer 2014 to summer 2015 period suggests the supply of volcanic products emitted from the eruption of Bárðarbunga in Holuhraun, Iceland, which started in the summer of 2014 (Schmidt *et al.*, 2015). SO_4^{2-} and F^- concentrations in Icelandic precipitation were about 20 times higher after the eruption than before due to the contribution of volcanic SO_2 and HF (Stefansson *et al.*, 2017). Therefore, the supply of volcanic products emitted from the volcanic eruption could have greatly increased the SO_4^{2-} and F^- concentrations in the snow on the Greenland ice sheet. The layers in the summer 2014 to summer 2015 period would have been affected by volcanic products derived from the eruption. Previous snow pit studies at EGRIP (Du *et al.*, 2019a, 2019b) also found increases of $nssSO_4^{2-}$, F^-, and non-sea salt S concentrations in the layers during

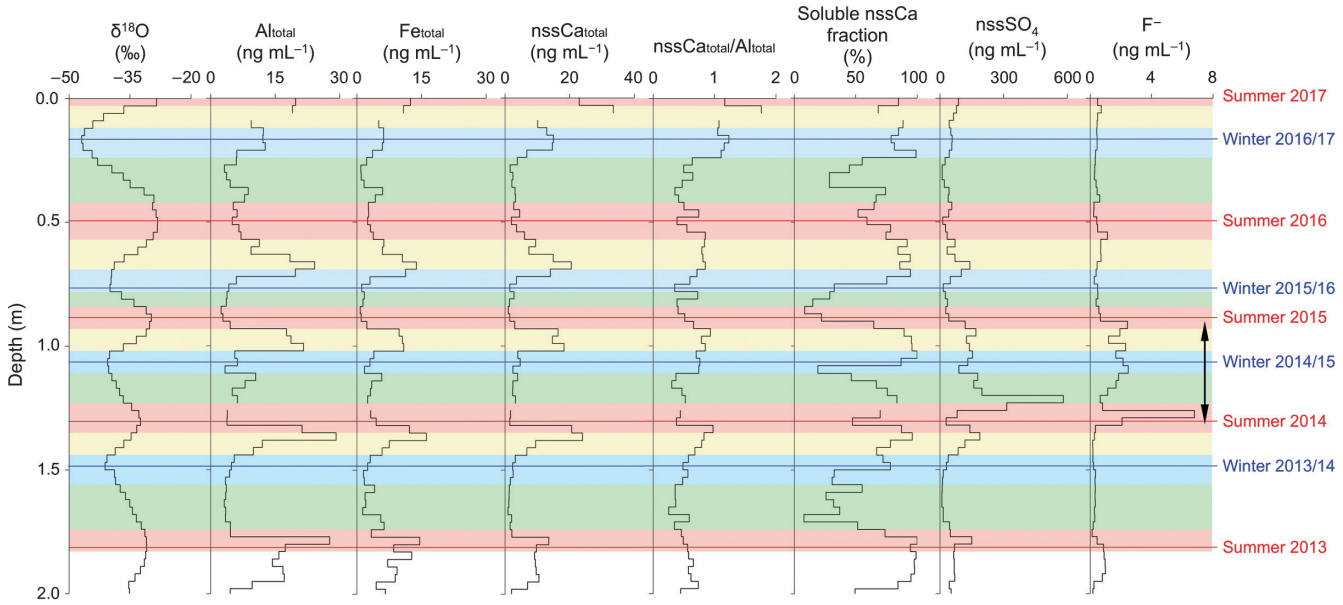

Fig. 2. Depth profiles of the metallic elements, $nssCa_{total}/Al_{total}$ ratio, soluble nssCa fraction, $nssSO_4^{2-}$, and F^-, along with that of $\delta^{18}O$ from Komuro *et al.* (2021). The red and blue lines indicate the center depths of summer and winter, respectively, for each year. The yellow, red, green and blue areas indicate the spring, summer, autumn and winter layers, respectively. The black bidirectional arrow indicates the period summer 2014 to summer 2015 (volcanic period).

this period, and attributed them to volcanic products from the Bárðarbunga eruption. Du *et al.* (2019b) found that rare earth element patterns in the layers during the summer 2014 to summer 2015 period were similar to those of volcanic products emitted from 2014–2015 eruption of Bárðarbunga. In the following discussion, we call the summer 2014 to summer 2015 period the volcanic period and the other periods non-volcanic periods.

The seasonal variations of Al_{total}, Fe_{total}, and $nssCa_{total}$ concentrations indicate seasonal variation of mineral particle concentrations with spring maxima (Fig. 2). Although the volcanic products could be another source of Al, Fe, and Ca in the volcanic period, the seasonality of Al_{total}, Fe_{total}, and $nssCa_{total}$ concentrations in this period was same as those in the non-volcanic periods. Moreover, the averages of Al_{total}, Fe_{total}, and $nssCa_{total}$ concentrations in the volcanic period (8.83, 4.98, and 6.08 ng mL^{-1}) did not exceed those for 2013–2017 (9.47, 5.39, and 7.11 ng mL^{-1}). Therefore, volcanic products from the 2014–2015 eruption of Bárðarbunga probably had little effect on those metallic element concentrations.

The seasonal variation of the $nssCa_{total}/Al_{total}$ ratio indicates that the Ca content in mineral particles increased in winter–spring and decreased in summer–autumn (Fig. 2). The soluble nssCa fraction was also higher in winter–spring; therefore, the increase of Ca content in those seasons was probably due to an increase of soluble Ca. The seasonal variations of soluble Ca content in mineral particles suggests that their major source region also varied seasonally. In autumn 2014, the $nssCa_{total}/Al_{total}$ ratio did not increase; only the soluble nssCa fraction increased. Thus, this increase in soluble nssCa fraction was not due to mineral particle supplies from source regions with high soluble Ca content, as observed in winter–spring of other years. Because autumn 2014 is part of the volcanic period, it is possible that volcanic acids from the 2014–2015 eruption of Bárðarbunga leached Ca from insoluble mineral particles and increased the soluble nssCa fraction.

Mineral particle concentrations for 2013–2017 calculated from the Al_{total} concentrations ranged from 29 to 354 μg kg^{-1} with an average of 115 ± 82 μg kg^{-1} (unless otherwise noted, uncertainties here are the standard deviation). Although recent observations of mineral particle concentrations in inland regions of Greenland are limited, Carmagnola *et al.* (2013) reported mineral particle concentrations from 49 to 310 μg kg^{-1} with an average value of 138 ± 69 μg kg^{-1} for May and June 2011 at Summit. The average concentration of mineral particles in this study was not significantly different from that in the previous study. The 4-year average of annual mineral particle fluxes (summer 2013 to summer 2017) at EGRIP calculated using accumulation rates reported by Komuro *et al.* (2021) was 16.5 mg m^{-2} yr^{-1}. This was within the range of fluxes at the inland sites of the Greenland ice sheet (GRIP, NGRIP, and Dye-3) (14–19 mg m^{-2} yr^{-1}) reported by Bory *et al.* (2003b).

Du *et al.* (2019b) reported average concentrations of water- and acid-soluble Fe of 0.252 and 2.17 ng g^{-1}, respectively, for 2012–2017 at EGRIP. The average Fe_{total} concentration for 2013–2017 in this study (5.39 ng mL^{-1}) was 21 and 2.5 times the concentrations of water- and acid-soluble Fe, respectively. The majority of Fe in snow is present as insoluble fractions and even leaching treatment by acidification cannot extract total Fe in snow (*e.g.*, Gaspari *et al.*, 2006). Thus, the reason for higher average Fe concentrations in the present study than in the previous study is that we extracted total Fe from snow samples by the acid decomposition method. The comparison of this study with the previous study suggests that the average percentages in water- and acid-soluble Fe are approximately 5 % and 40 %, respectively, in recent snow at EGRIP.

3.2 Insoluble particle concentration

The depth profile for insoluble particle concentration for the entire size range measured in this study (0.52–12 μm) along with the $\delta^{18}O$ and Al_{total} concentration profiles are shown in Fig. 3. The insoluble particle concentration showed a seasonal variation, which was similar to that of Al_{total} concentrations. However, in the volcanic period, the peak depth of the insoluble particle concentration (0.90–0.99 m) did not match that of the Al_{total} concentration (0.93–1.02 m). The correlation between Al_{total} and insoluble particle concentrations was moderate for 2013–2017 (r=0.78, p<0.001) (Fig. 4). The correlation was stronger for the non-volcanic periods (r=0.88, p<0.001) and weaker for the volcanic period (r=0.49, p<0.1). In non-volcanic periods, the correlation was stronger (r=0.94, p<0.001) if the sample from 0.03–0.06 m depth was excluded as an outlier.

The strong correlation for the non-volcanic periods indicates that the insoluble particles were mainly mineral particles for those periods. The weak correlation for the volcanic period may be caused by inputs of volcanic products from the 2014–2015 eruption of Bárðarbunga. Volcanic glasses, which are an Al-free volcanic product, increase only the insoluble particle concentration. Furthermore, dissolution of mineral particles by volcanic H_2SO_4 and HF can decrease the insoluble particle concentrations but does not change the Al_{total} concentration because Al ions from these particles are also reflected in the Al_{total} concentration. Therefore, the input of volcanic products can explain the changes in insoluble particle concentration without changes in the Al_{total} concentration and can also explain the weak correlation between the two concentrations for the volcanic period.

In the sample from 0.03–0.06 m depth, the insoluble particle concentration appeared to be too high compared with the Al_{total} concentration (Figs. 3 and 4). The insoluble particle concentration in this layer (98.4×10^3 μm^3 mL^{-1}) was approximately twice that estimated from the regression line in the non-volcanic periods (47.8×10^3 μm^3 mL^{-1}) (Fig. 4). Thus, this layer likely contained Al-free insoluble

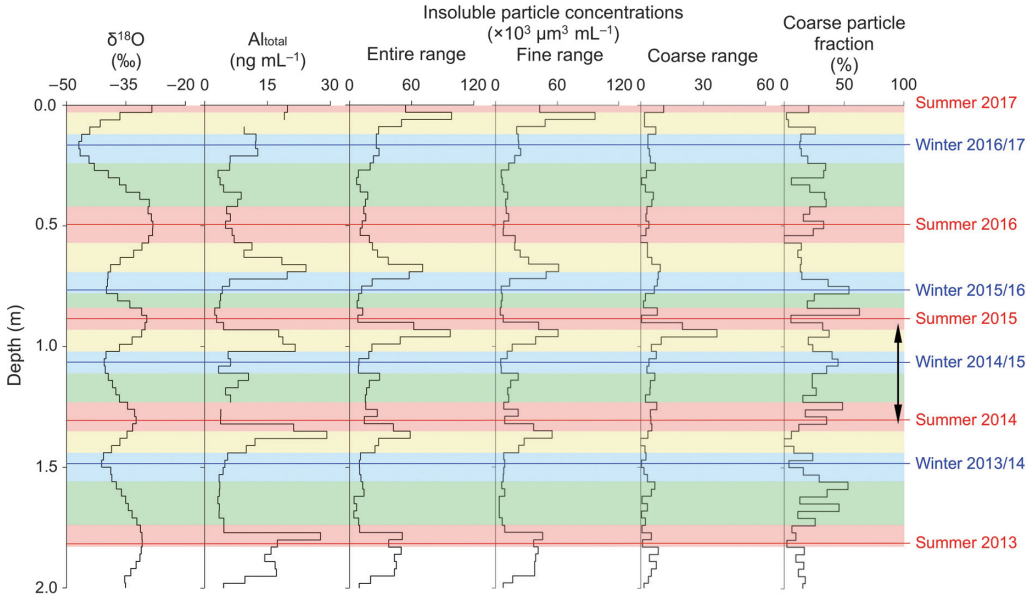

Fig. 3. Depth profiles of insoluble particle concentrations and coarse particle fraction along with those of $\delta^{18}O$ and Al_{total}. The $\delta^{18}O$ profile is from Komuro *et al.* (2021). The insoluble particle concentrations are shown for the entire range (0.52–12 μm), fine range (0.52–5 μm), and coarse range (5–12 μm). The red and blue lines indicate the center depths of summer and winter, respectively, for each year. The yellow, red, green and blue areas indicate the spring, summer, autumn and winter layers, respectively. The black bidirectional arrow indicates the period summer 2014 to summer 2015 (volcanic period).

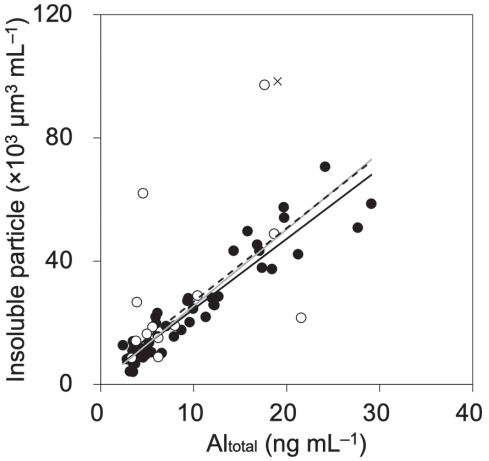

Fig. 4. Relationship between concentrations of Al_{total} and insoluble particles for the entire size range. The open and filled circles denote data from the summer 2014 to summer 2015 period (volcanic period) and the other periods (non-volcanic periods), respectively. The cross shows an outlier in the non-volcanic periods (sample from 0.03–0.06 m depth). The black dashed line is the regression line for the data for 2013–2017. The grey line is the regression line for the non-volcanic periods with the outlier. The black solid line is the regression line for the data in the non-volcanic periods without the outlier.

particles. This layer was within the non-volcanic periods and unlikely to be affected by the volcanic products. The reason for the anomalous insoluble particle concentration in this layer was unclear in this study.

3.3 *Particle size distribution*

Average size distributions of insoluble particle concentrations for 2013–2017 and non-volcanic periods are shown in Fig. 5. These average size distributions showed a unimodal distribution with mode diameters of around 2 μm. This distribution is also reported from previous ice core studies in the inland regions of the Greenland ice sheet (GRIP and NGRIP) (Steffensen, 1997; Ruth *et al.*, 2003).

In previous studies, mineral particles larger than 5 μm in diameter were treated as originating from soil regions near the Greenland ice sheet (local sources) (Amino *et al.*, 2021; Nagatsuka *et al.*, 2021). Thus, we divided the insoluble particle concentration data into fine and coarse particles with a boundary of 5 μm to examine seasonal variations of the contribution from distant and local sources (Fig. 3). The concentration of fine particles (0.52–5 μm) showed a seasonal variation with maxima in spring, as did the concentration of particles over the entire size range. The concentration of coarse particles varied from layer to layer, however, the seasonal averages of the concentration in the non-volcanic periods were similar ($3.24–4.18 \times 10^3$ μm^3 mL^{-1}). This difference in seasonality suggests that the seasonality of mineral particle supply from local sources differed from that from distant sources. The volume fractions of coarse particles in the entire size range (coarse particle fraction) decreased in winter–spring and increased in summer–autumn in the non-volcanic periods. These changes suggest that the fraction of mineral particles from distant sources increased in winter–spring, whereas that from local sources increased in summer–autumn.

3.4 *Characteristic estimation of mineral particles from distant and local sources*

To estimate the Ca/Al ratios of mineral particles from distant and local sources, we examined the relationship between the coarse particle fraction and $nssCa_{total}/Al_{total}$ ratio (Fig. 6 and Table 1). In non-volcanic periods, the $nssCa_{total}/Al_{total}$ ratio averages increased with decreasing coarse particle fraction. The average $nssCa_{total}/Al_{total}$ ratio for low coarse particle fractions (<20 %) was roughly 1.5 times the crustal average Ca/Al ratio (0.50) (Taylor, 1964). This result remained the same even when an outlier in the non-volcanic period (sample from 0.03–0.06 m depth; see Section 3.2) was excluded, suggesting that the mineral particles from distant sources had higher Ca/Al ratios than the crustal average. The average $nssCa_{total}/Al_{total}$ ratio for high coarse particle fractions (>40 %) was 0.7 times the crustal average, suggesting that mineral particles from local sources had the same or lower Ca/Al ratios than the crustal average. As well as the $nssCa_{total}/Al_{total}$ ratio, the average soluble nssCa fraction increased with the decrease of coarse particle fraction (Table 1), suggesting that the higher $nssCa_{total}/Al_{total}$ ratios of mineral particles from distant sources were due to their higher soluble Ca contents. These relationships were unclear in the volcanic period, possibly due to the contributions of volcanic products from the 2014–2015 eruption of Bárðarbunga in this period. In Section 3.6, we discuss the source regions of mineral particles in more detail using the $nssCa_{total}/Al_{total}$ ratios obtained from these analyses.

The Fe_{total}/Al_{total} ratio in non-volcanic periods showed no significant changes with the changes in the coarse

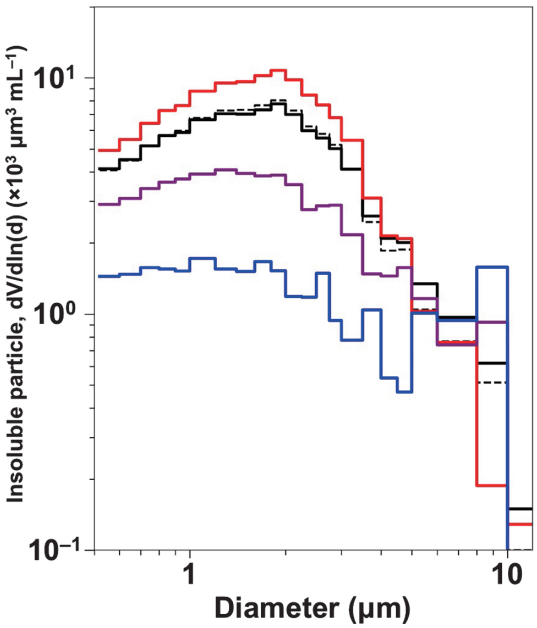

Fig. 5. Average size distributions of insoluble particles by volume. The black and dashed lines show the average for 2013–2017 and the non-volcanic periods, respectively. The red, purple, and blue lines show the averages for low (<20 %), moderate (20 %–40 %), and high (>40 %) coarse particle fraction ranges for the non-volcanic periods, respectively.

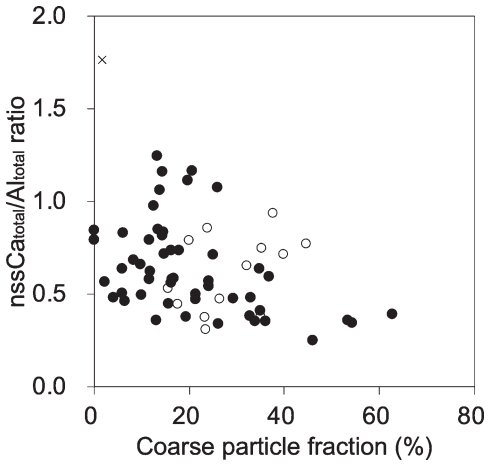

Fig. 6. Relationship between coarse particle fraction and $nssCa_{total}/Al_{total}$ ratio. The open and filled circles denote data during the summer 2014 to summer 2015 period (volcanic period) and the other periods (non-volcanic periods), respectively. The cross shows an outlier in the non-volcanic periods (sample from 0.03–0.06 m depth).

Table 1. Averages and standard deviations of $nssCa_{total}/Al_{total}$, Fe_{total}/Al_{total}, and soluble nssCa fractions for low (<20 %), moderate (20 %–40 %), and high (>40 %) coarse particle fraction ranges.

Coarse particle fraction	Non-volcanic period			Volcanic period		
	$nssCa_{total}/Al_{total}$	Fe_{total}/Al_{total}	Soluble nssCa fraction (%)	$nssCa_{total}/Al_{total}$	Fe_{total}/Al_{total}	Soluble nssCa fraction (%)
Low	0.75 ± 0.29 (0.72 ± 0.22)	0.60 ± 0.26	73 ± 27 (73 ± 28)	0.49 ± 0.04	0.61 ± 0.22	77 ± 7
Moderate	0.57 ± 0.23	0.55 ± 0.23	58 ± 20	0.62 ± 0.21	0.62 ± 0.20	70 ± 25
High	0.34 ± 0.05	0.52 ± 0.36	33 ± 17	0.77[a]	0.48[a]	87[a]

The values in parentheses show the average and standard deviation of the data with an outlier (sample from 0.03–0.06 m depth) excluded from the non-volcanic periods.

[a] $nssCa_{total}/Al_{total}$, Fe_{total}/Al_{total}, and soluble nssCa fractions of a single datum are shown because this range in the volcanic period has only one datum.

particle fraction (Table 1), indicating that there was no significant difference in Fe/Al ratios between mineral particles from distant and local sources.

Figure 5 shows the average size distribution of insoluble particle concentrations for each coarse particle fraction in non-volcanic periods. The average size distribution for the low coarse particle fraction had a clear unimodal distribution with a mode diameter of around 2 μm, showing that mineral particles from distant sources had a unimodal distribution with a mode diameter of around 2 μm, as reported previously (Steffensen *et al.*, 2001; Bory et al., 2003b). However, the unimodal distribution became unclear as the coarse particle fraction increased, suggesting a difference in the size distributions of mineral particles from distant and local sources. The average size distribution for the high coarse particle fraction suggests that for the mineral particles transported from local sources to EGRIP, as the particle size increased, the particle concentration changed little for 0.52–2 μm particles, decreased for 2–5 μm particles, and increased again for 5–10 μm particles.

3.5 *Source estimation of coarse mineral particles using back-trajectory analysis*

To estimate the local source regions, the origin of coarse mineral particles, we calculated the probability distribution of air masses arriving at EGRIP for 2013–2017 (Fig. 7a). The atmospheric residence time of particles larger than 5 μm is roughly 3 days or less (Tegen and Lacis, 1996); therefore, we show the distribution of the 3-day backward trajectories. To calculate regional contributions of the air masses, land regions were divided into the Greenland coast, Canada (including Alaska), Iceland, and northern Eurasia (Europe and Russia) (Fig. 7b). The regional contributions of the air masses were calculated as averages for annual (January-December), spring (March-May), summer (June-August), autumn (September-November), and winter (December-February) (Fig. 7c). The calculation results show that the air masses in the range of 0–1500 m a.g.l. that reached EGRIP came mainly from the coastal regions in Greenland, and that the contribution from other regions was small (Fig. 7a). The contribution from the Greenland coast was 88 %–92 % and the remainder from the rest of the regions was <12 % (Fig. 7c). The seasonal contribution from the Greenland coast showed a maximum in spring and a minimum in autumn; however, the range of variation was small (4 %). These results indicate that the local source regions for the coarse mineral particles were primarily the Greenland coast in all seasons.

To examine the local source regions in more detail, the regional contribution of the air masses for the coasts in Greenland was calculated (Fig. 8). The probability distribution of the air masses over the Greenland coast shows that they came mainly from the western and eastern coasts in central Greenland (coasts between 64° N and 76° N), and rarely from the northern and southern coasts in Greenland (coasts above 76° N and below 64° N,

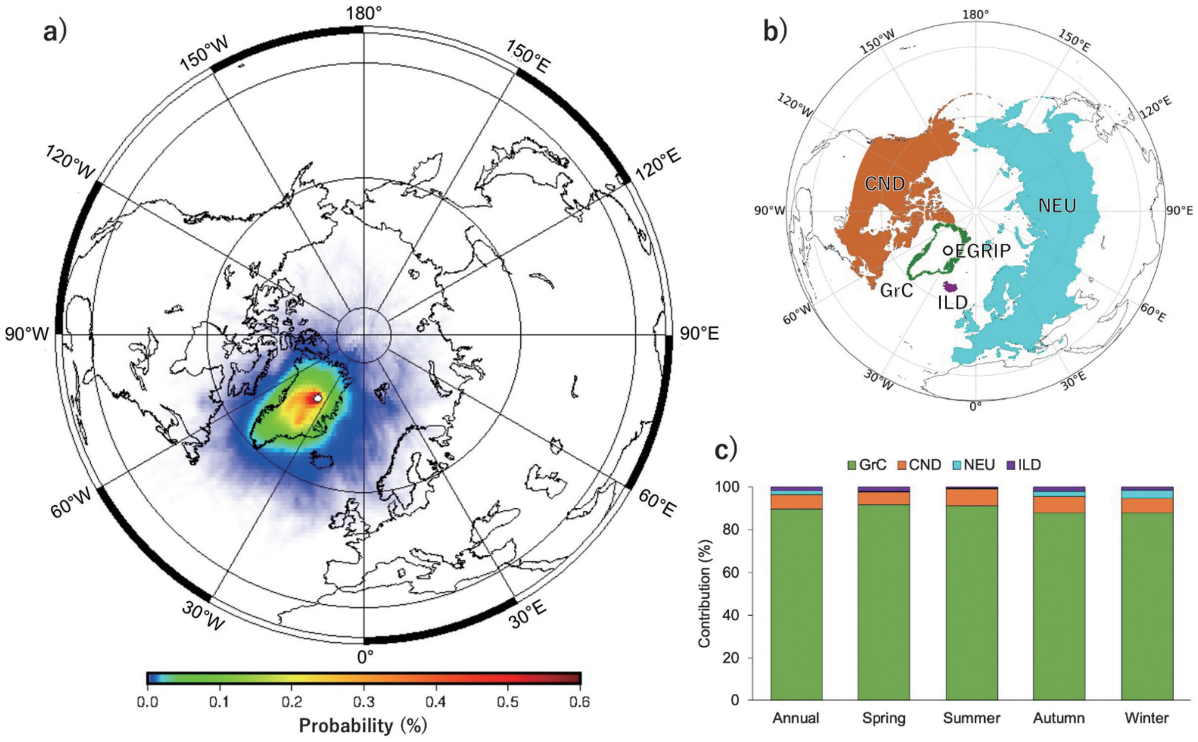

Fig. 7. (a) Probability distribution of air masses arriving at EGRIP from a 3-day three-dimensional back-trajectory analysis for 2013–2017. (b) Four regions used for calculating regional contributions (GrC: Greenland coast, green; CND: Canada and Alaska, orange; NEU: northern Eurasia, light blue; ILD: Iceland, purple). (c) Annual and seasonal averages of the contributions from the four regions.

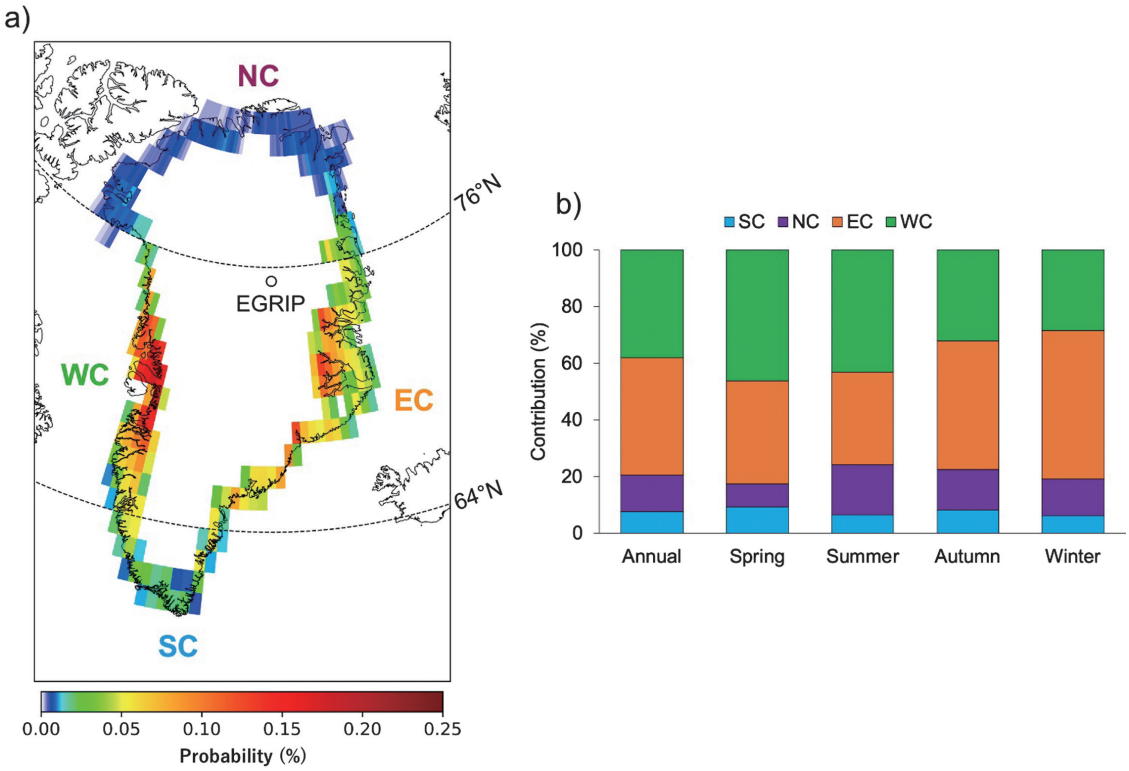

Fig. 8. (a) Probability distribution of the air masses in the Greenland coasts for 2013–2017 and four coastal regions used for calculating regional contributions (WC: western coast, EC: eastern coast, NC: northern coast, SC: southern coast). The 76°N and 64°N lines are the boundary between the northern coast and the eastern/western coasts, and between the southern coast and the eastern/western coasts, respectively. (b) Annual and seasonal averages of the contribution for the four coastal regions.

respectively) (Fig. 8a). Calculating the regional contributions of the air masses for these coasts shows that the contributions of western and eastern coasts (29 %–46 % and 33 %–52 %) were similar (Fig. 8b). The sum of contributions for the western and eastern coasts was 80 % for the all-season average with a small seasonal variation (<4 % from the average). These results suggest that the local source regions were primarily the western and eastern coasts in central Greenland in all seasons.

3.6 Possible source regions of mineral particles and their seasonal changes

Bory *et al.* (2003b) pointed out that nearly uniform annual fluxes of mineral particles in the inland regions (GRIP, NGRIP, and Dye-3) are due to the long-distant transported fine mineral particles that fall uniformly on the ice sheet from high elevations. Thus, the similarity of the annual fluxes between EGRIP and these inland regions (see Section 3.1) is evidence that the mineral particles deposited at EGRIP could come mainly from distant regions. Additionally, the average particle size distribution for 2013–2017 was the unimodal distribution (see Section 3.3), which is interpreted as the signature of mineral particles from distant source regions to the Greenland ice sheet (Simonsen *et al.*, 2019), also suggesting that the mineral particles could come mainly from distant regions.

In addition to fine mineral particles, we observed coarse mineral particles (see Section 3.3). The presence of coarse mineral particles indicates that there were also local mineral particle sources. The back trajectory analysis suggested that the local source regions were primarily the western and eastern coasts of central Greenland (see Section 3.5). The coarse mineral particle concentration varied from layer to layer (see Section 3.3), thus, it is suggested that the mineral particle supply from the coastal regions varied with time. Although the intra-annual variation in dust event days in the western coast (Kangerlussuaq) is reported by a previous study (Bullard and Mockford, 2018), the seasonal average of coarse mineral particle concentration in this study varied little. The variation of dust event days is close to a monthly scale; thus, the coarse particle concentrations averaged by seasons were possibly unable to capture the variation.

The increase in fine particle concentration and decrease in coarse particle fraction (*i.e.*, increase in fine particle fractions) in winter–spring (see Section 3.3) suggest that the contribution of fine mineral particles from distant regions is large in those seasons. Bory *et al.* (2003a) found that the strontium/neodymium isotopic ratios of mineral particles in spring at Summit could be explained by those of arid regions in Asia. Thus, the fine mineral particles found in winter–spring in this study could also have originated from the Asian arid regions. In

general, Ca/Al ratios of soils in arid regions are higher than that of the crustal average due to the abundance of calcium salts, such as calcite. The Ca/Al ratios of Asian soils are in the range of 0.31–4.14 (Formenti *et al*., 2011). Asian mineral aerosols in the North Pacific (Mauna Loa) have a Ca/Al ratio of 0.99 ± 0.71 during the season of high mineral aerosol concentrations (around spring) (Holmes and Zoller, 1996). These Ca/Al ratio ranges in Asian mineral particles can explain the $nssCa_{total}/Al_{total}$ ratios for the low coarse particle fractions in this study (Table 1). Similarly, the Fe/Al ratio range in the Asian source regions (0.36–1.74) (Formenti *et al*., 2011) can also explain the Fe_{total}/Al_{total} ratios for the low coarse particle fractions. The Sahara is also proposed as an additional distant arid source of mineral particles transported to Greenland (Lupker *et al*., 2010); however, the Ca/Al ratio in the Sahara (0.36–0.92) (Formenti *et al*., 2011) cannot fully explain the $nssCa_{total}/Al_{total}$ ratios with the low coarse particle fractions. The mineral particle emissions from the Sahara increase in spring and summer (Laurent *et al*., 2008), which cannot explain the increased contribution of fine mineral particles in winter–spring in this study. Therefore, the Asian arid regions are more plausible for explaining our results.

Calcium salts contained in the soils of arid regions are soluble; thus, the higher Ca solubility in distant source mineral particles (see Section 3.4) is explained by the contribution of the calcium salts. The increase in soluble Ca content in winter–spring supports a strong contribution from mineral particles originating from arid regions in those seasons.

The characteristics of mineral particles in summer–autumn suggest that the main source regions of mineral particles in this season were different from those in winter–spring. Bory *et al*. (2003a) suggested that the mineral particles at Summit came from the arid regions in Asia not only in spring, but also in the other seasons. However, the increase in coarse particle fraction in summer–autumn (see Section 3.3) cannot be explained by the mineral particles transported from distant source regions, such as Asia. In summer–autumn, the relative contributions of mineral particles from the western and eastern coasts in central Greenland probably increased due to the decrease in supply of fine mineral particles from distant arid regions.

The direct comparison of the elemental compositions of mineral particles in this study and soils in the western and eastern coasts in central Greenland was difficult because the information about the composition of the soils is poor. However, the accumulation of calcium salts requires high air temperatures and low precipitation (Zhu *et al*., 2012), as found in Asian arid regions, whereas the coastal regions in Greenland have lower temperatures and receive more precipitation than arid regions (Cappelen, 2018; Li *et al*., 2012). Therefore, the soils in the Greenland coasts probably do not accumulate calcium salt minerals and the soil Ca content and solubility may be low compared with distant arid regions. An X-ray absorption near-edge structure spectroscopy study of soils in the eastern coast (around SE-Dome) suggested that calcite and gypsum contributed little to the soil spectra (Miyamoto *et al*., 2022). Wientjes *et al*. (2011) reported the mineralogical and elemental compositions of mineral particles deposited on the western coastal region of the Greenland ice sheet and concluded that the particles likely originated from the coastal soils on west Greenland. The Ca/Al and Fe/Al ratios reported by Wientjes *et al*. (2011) (0.38–0.51 and 0.53–0.61) were close to the ratios of $nssCa_{total}/Al_{total}$ and Fe_{total}/Al_{total} in the layers with high coarse particle fractions, respectively (Table 1). This result supports the hypothesis that the western coast was a main local source of mineral particles containing coarse particles to EGRIP. For the eastern coast, we could not perform a comparative analysis similar to that for the western coast because of the poor observation data for mineral particles from the eastern coast. In future work, we will perform time-series comparisons of atmospheric and ground surface conditions for the Greenland coasts and mineral particles deposited in EGRIP to understand their local sources better.

4. Conclusion

At EGRIP, the Al_{total}, Fe_{total}, and Ca_{total} concentrations showed clear seasonality. These concentrations increased in spring, indicating an increase in mineral particle concentrations. Volcanic products came from the 2014–2015 eruptions of Bárðarbunga, Iceland, and likely had little effect on the concentrations of these metallic elements. The depth profile of insoluble particle concentrations was similar to that of the Al_{total} concentrations, suggesting that a large fraction of the insoluble particle volumes in snow at EGRIP consisted of mineral particles. The supply of volcanic products may explain the discrepancy between the depth profiles of Al_{total} and insoluble particle concentrations in the summer 2014 to summer 2015 layers.

The average annual fluxes and size distributions of mineral particles in this study matched those from the other inland sites on the Greenland ice sheet reported in previous studies. Thus, a large proportion of the mineral particles deposited at EGRIP may have the same origin as those at other inland sites on the Greenland ice sheet and may have come from distant regions. However, the coarse mineral particles contained in the snow at EGRIP suggested that nearby soil regions also supplied mineral particles. The back trajectory analysis suggested that the nearby source regions were primarily the western and eastern coasts of central Greenland. The decrease in coarse particle fraction (*i.e*., the increase in fine particle fraction) in winter–spring likely indicated that the relative contribution of mineral particles transported from distant regions increased in those seasons. The

increase in average $nssCa_{total}/Al_{total}$ ratio and soluble nssCa fraction with the increase in fine particle fraction suggested that the mineral particles from distant regions came from arid soil regions, such as those in Asia, which contain a large fraction of calcium salts. In contrast, in summer–autumn, the coarse particle fraction increased and the $nssCa_{total}/Al_{total}$ ratio and soluble nssCa fraction decreased, suggesting that the relative contribution of mineral particles transported from the western and eastern coasts increased in summer–autumn. In future work, we will investigate atmospheric and ground surface conditions using resources such as satellite observations and reanalysis data to reveal the cause of temporal variations in the concentrations, fluxes, and source regions of mineral particles. Additionally, we will analyze ice core data at EGRIP to understand longer-term variations in the factors affecting mineral particles in the inland regions.

Acknowledgements

EGRIP is directed and organized by the Center of Ice and Climate at the Niels Bohr Institute and US NSF, Office of Polar Programs. It is supported by funding agencies and institutions in Denmark (A. P. Møller Foundation, UCPH), the US (US NSF, Office of Polar Programs), Germany (AWI), Japan (NIPR and ArCS), Norway (BFS), Switzerland (SNF), France (IPEV, IGE), and China (CAS). We are grateful to Kaori Fukuda, Maki Nakatani, and Hiromi Okumura at NIPR for laboratory measurements. We also thank Sakiko Ishino at NIPR for helpful comments. This research was supported by the Arctic Challenge for Sustainability (ArCS) Project (Program Grant Number JPMXD1300000000), the Arctic Challenge for Sustainability II (ArCS II) (Program Grant Number JPMXD1420318865), the Environment Research and Technology Development Funds (JPMEERF20172003, JPMEERF20202003, and JPMEERF20232001) of the Environmental Restoration and Conservation Agency of Japan, the National Institute of Polar Research (Project Research KP305), and JSPS KAKENHI (Grant Numbers 18H04140, 20K19962, and 20K19962).

References

Amino, T., Iizuka, Y., Matoba, S., Shimada, R., Oshima, N., Suzuki, T., Ando, T., Aoki, T., and Fujita, K. (2021): Increasing dust emission from ice free terrain in southeastern Greenland since 2000. *Polar Sci.*, **27**, 100599, doi:10.1016/j.polar.2020.100599.

Baccolo, G., Delmonte, B., Albani, S., Baroni, C., Cibin, G., Frezzotti, M., Hampai, D., Marcelli, A., Revel, M., Salvatore, M. C., Stenni, B. and Maggi, V. (2018): Regionalization of the Atmospheric Dust Cycle on the Periphery of the East Antarctic Ice Sheet Since the Last Glacial Maximum. *Geochem., Geophys., Geosyst.*, **19**, 3540–3554, doi:10.1029/2018GC007658.

Biscaye, P. E., Grousset, F. E.,Revel, M., Van Der Gaast, S., Zielinski, G. A., Vaars, A. and Kukla, G. (1997): Asian provenance of glacial dust (stage 2) in the Greenland Ice Sheet Project 2 Ice Core, Summit, Greenland. *J. Geophys. Res.: Oceans*, **102** (C12), 26765–26781, doi:10.1029/97JC01249.

Bory, A. J.-M., Biscaye, P. E. and Grousset, F. E. (2003a): Two distinct seasonal Asian source regions for mineral dust deposited in Greenland (NorthGRIP). *Geophys. Res. Lett.*, **30** (4), doi:10.1029/2002GL016446.

Bory, A. J. -M., Biscaye, P. E., Piotrowski, A. M. and Steffensen, J. P. (2003b): Regional variability of ice core dust composition and provenance in Greenland. *Geochem., Geophys. Geosyst.*, **4** (12), 1107, doi:10.1029/2003GC000627.

Broecker, W. S. and Peng, T. H. (1982): Tracers in the sea. *Eldigio Press*, Lamont-Doherty Earth Observatory of Columbia University, Palisades, NY, 1–690.

Bullard, J. E. and Mockford, T. (2018): Seasonal and decadal variability of dust observations in the Kangerlussuaq area, west Greenland. *Arct. Antarct. Alp. Res.*, **50** (1), doi:10.1080/15230430.2017.1415854.

Cappelen, J. (Ed.) (2018): Greenland - DMI Historical Climate Data Collection 1784–2017, *DMI Report 18-04*, DMI, Copenhagen, Denmark.

Carmagnola, C. M., Domine, F., Dumont, M., Wright, P., Strellis, B., Bergin, M., Dibb, J., Picard, G., Libois, Q., Arnaud, L. and Morin, S. (2013): Snow spectral albedo at Summit, Greenland: measurements and numerical simulations based on physical and chemical properties of the snowpack. *The Cryosphere*, **7**, 1139–1160, doi:10.5194/tc-7-1139-2013.

Dibb, J. E., Whitlow, S. I. and Arsenault, M. (2007): Seasonal variations in the soluble ion content of snow at Summit. Greenland: Constraints from three years of daily surface snow samples. *Atmos. Environ.*, **41** (24), 5007–5019, doi:10.1016/j.atmosenv.2006.12.010.

Du, Z., Xiao, C., Zhang, Q., Li, C., Wang, F., Liu, K. and Ma, X. (2019a): Climatic and environmental signals recorded in the EGRIP snowpit, Greenland. *Environ. Earth Sci.*, **78** (5), 1–10, doi:10.1007/s12665-019-8177-4.

Du, Z., Xiao, C., Zhang, Q., Handley, M. J., Mayewski, P. A. and Li, C. (2019b): Relationship between the 2014–2015 Holuhraun eruption and the iron record in the East GRIP snow pit. *Arct. Antarct. Alp. Res.*, **51** (1), 290–298, doi:10.1080/15230430.2019.1634441.

Formenti, P., Schütz, L., Balkanski, Y., Desboeufs, K., Ebert, M., Kandler, K., Petzold, A., Scheuvens, D., Weinbruch, S. and Zhang, D. (2011): Recent progress in understanding physical and chemical properties of African and Asian mineral dust. *Atmos. Chem. Phys.*, **11**, 8231–8256, doi:10.5194/acp-11-8231-2011.

Gaspari, V., Barbante, C., Cozzi, G., Cescon, P., Boutron, C. F., Gabrielli, P., Capodaglio, G., Ferrari, C., Petit, J. R. and Delmonte, B. (2006): Atmospheric iron fluxes over the last deglaciation: Climatic implications. *Geophys. Res. Lett.*, **336** (L03704), doi:10.1029/2005GL024352.

Holmes, J. and Zoller, W. (1996): The elemental signature of transported Asian dust at Mauna Loa observatory. *Tellus B*, **48** (1), 83–92, doi:10.3402/tellusb.v48i1.15669.

Kalnay, E., Kanamitsu, M., Kistler, R., Collins, W., Deaven, D., Gandin, L., Iredell, M., Saha, S., White, G., Woollen, J., Zhu, Y., Chelliah, M., Ebisuzaki, W., Higgins, W., Janowiak, J., Mo, K. C., Ropelewski, C., Wang, J., Leetmaa, A., Reynolds, R., Jenne, R., Joseph, D. (1996): The NCEP/NCAR 40-Year Reanalysis Project. *Bull. Am. Meteorol. Soc.*, **77**, 437–472, doi:10.1175/1520-0477(1996)077<0437:TNYRP>2.0.CO;2.

Kjær, H. A., Zens, P., Black, S., Lund, K. H., Svensson, A. and Vallelonga, P. (2022): Canadian forest fires, Icelandic volcanoes and increased local dust observed in six shallow Greenland firn cores. *Clim. Past*, **18**, 2211–2230, doi:10.5194/cp-18-2211-2022, 2022.

Komuro, Y., Nakazawa, F., Hirabayashi, M., Goto-Azuma, K., Nagatsuka, N., Shigeyama, W., Matoba, S., Homma, T., Steffensen, J. P. and Dahl-Jensen, D. (2021): Temporal and spatial variabilities in surface mass balance at the EGRIP site, Greenland from 2009 to 2017. *Polar Sci.*, **27**, 100568, doi:10.1016/j.polar.2020.100568.

Kuramoto, T., Goto-Azuma, K., Hirabayashi, M., Miyake, T.,

Motoyama, H., Steffensen, J. P. and Dahl-Jensen, D. (2011): Seasonal variations of snow chemistry at NEEM, Greenland. *Ann. Glaciol.*, **52** (58), 193–200, doi:10.3189/172756411797252365.

Laurent, B., Marticorena, B., Bergametti, G., Leon, J.F., Mahowal, N.M. (2008): Modeling mineral dust emissions from the Sahara desert using new surface properties and soil database. *J. Geophys. Res.:Atmos.*, **113**, D14218, doi:10.1029/2007JD009484.

Li, B., Chen, Y., Shi, X., Chen, Z. and Li, W. (2012) Temperature and precipitation changes in different environments in the arid region of northwest China. *Theor. Appl. Climatol.*, **112** (3–4), 589–596, doi:10.1007/s00704-012-0753-4.

Lupker, M., Aciego, S. M., Bourdon, B., Schwander, J. and Stockerc, T.F. (2010): Isotopic tracing (Sr, Nd, U and Hf) of continental and marine aerosols in an 18th century section of the Dye-3 ice core (Greenland). *Earth Planet. Sci. Lett.*, **295** (1–2), 277–286, doi:10.1016/j.epsl.2010.04.010.

Miyamoto, C., Iizuka, Y., Matoba, S., Hattori, S. and Takahashi, Y. (2022): Gypsum formation from calcite in the atmosphere recorded in aerosol particles transported and trapped in Greenland ice core sample is a signature of secular change of SO2 emission in East Asia. *Atmos. Environ.*, **278** (1), 119061–119061, doi:10.1016/j.atmosenv.2022.119061.

Nagatsuka, N., Goto-Azuma, K., Tsushima, A., Fujita, K., Matoba, S., Onuma, Y., Dallmayr, R., Kadota, M., Hirabayashi, M., Ogata, J., Ogawa-Tsukagawa, Y., Kitamura, K., Minowa, M., Komuro, Y., Motoyama, H. and Aoki, T. (2021): Variations in mineralogy of dust in an ice core obtained from northwestern Greenland over the past 100 years. *Clim. Past.*, **17**, 1341–1362, doi:10.5194/cp-17-1341-2021.

Nakazawa, F., Nagatsuka, N., Hirabayashi, M., Goto-Azuma, K., Steffensen, J. P. and Dahl-Jensen, D. (2021): Variation in recent annual snow deposition and seasonality of snow chemistry at the east Greenland ice core project (EGRIP) camp, Greenland. *Polar Sci.*, **27**, 100597, doi:10.1016/j.polar.2020.100597.

Ruth, U., Wagenbach, D., Bigler, M., Steffensen, J., Röthlisberger, R. and Miller, H. (2002): High-resolution microparticle profiles at NorthGRIP, Greenland: Case studies of the calcium–dust relationship. *Ann. Glaciol.*, **35**, 237–242, doi:10.3189/172756402781817347.

Ruth, U., Wagenbach, D., Steffensen, J. P. and Bigler, M. (2003): Continuous record of microparticle concentration and size distribution in the central Greenland NGRIP ice core during the last glacial period. *J. Geophys. Res.: Atmos.*, **108** (D3), 4098, doi:10.1029/2002JD002376.

Sato, H., Suzuki, T., Hirabayashi, M., Iizuka, Y., Motoyama, H. and Fujii, Y. (2013): Mineral and Sea-Salt Aerosol Fluxes over the Last 340 kyr Reconstructed from the Total Concentration of Al and Na in the Dome Fuji Ice Core. *Atmos. Clim. Sci.*, **3** (2), 186–192, doi:10.4236/acs.2013.32020.

Schmidt, A., Leadbetter, S., Theys, N., Carboni, E., Witham, C. S., Stevenson, J. A., Birch, C. E., Thordarson, T., Turnock, S., Barsotti, S., Delaney, L., Feng, W., Grainger, R. G., Hort, M. C., Höskuldsson, Á., Ialongo, I., Ilyinskaya, E., Jóhannsson, T., Kenny, P., Mather, T. A., Richards, N. A. D. and Shepherd, J. (2015): Satellite detection, long-range transport, and air quality impacts of volcanic sulfur dioxide from the 2014–2015 flood lava eruption at Bárðarbunga (Iceland). *J. Geophys. Res.: Atmos.*, **120**, 9739–9757, doi:10.1002/2015JD023638.

Simonsen, M. F., Baccolo, G., Blunier, T., Borunda, A., Delmonte, B., Frei, R., Goldstein, S., Grinsted, A., Kjær, H. A., Sowers, T., Svensson, A., Vinther, B., Vladimirova, D., Winckler, G., Winstrup, M. and Vallelonga, P. (2019): East Greenland ice core dust record reveals timing of Greenland ice sheet advance and retreat. *Nat. Commun.*, **10**, 1–8, doi:10.1038/s41467-019-12546-2.

Spolaor, A., Vallelonga, P., Gabrieli, J., Roman, M. and Barbante, C. (2013): Continuous flow analysis method for determination of soluble iron and aluminium in ice cores. *Anal. Bioanal. Chem.*, **405** (2–3), 767–74, doi:10.1007/s00216-012-6166-5.

Stefansson, A., Stefansdottir, G., Keller, N. S., Barsotti, S., Sigurdsson, A., Thorláksdóttir, S. B., Pfeffer, M.A., Eiriksdottir, E. S., Jonasdottir, E. B., Löwis, S. V. and Gislason, S. R. (2017): Major impact of volcanic gases on the chemical composition of precipitation in Iceland during the 2014–2015 Holuhraun eruption. J. *Geophys. Res.: Atmos.*, **122**, 1971–1982, doi:10.1002/2015JD024093.

Steffensen, J. P. (1997): The size distribution of microparticles from selected segments of the Greenland Ice Core Project ice core representing. *J. Geophys. Res.: Oceans*, **102** (C12), 26755–26763, doi:10.1029/97JC01490.

Steffensen, J. P., Andersen, M. L. S., Stampe, M. and Clausen, H. B. (2001): Microparticles, soil, derived chemical components and sea salt in the Hans Tausen Ice Cap ice core from Peary Island, North Greenland. *Medd. Grønland. Geosci.*, **39**, 151–160, doi:10.7146/moggeosci.v39i.140228.

Stein, A. F., Draxler, R. R., Rolph, G. D., Stunder, B. J. B., Cohen, M. D. and Ngan, F. (2015): NOAA's HYSPLIT atmospheric transport and dispersion modeling system. *Bull. Am. Meteorol. Soc.*, **96** (12), 2059–2077, doi:10.1175/BAMS-D-14-00110.1.

Svensson, A., Biscaye, P. E. and Grousset, F. E. (2000): Characterization of late glacial continental dust in the Greenland Ice Core Project ice core. *J. Geophys. Res.: Atmos.*, **105** (D4), 4637–4656, doi:10.1029/1999JD901093.

Taylor, S. R. (1964): Abundance of chemical elements in the continental crust: a new table. *Geochim. Cosmochim. Acta*, **28** (8), 1273–1285, doi:10.1016/0016-7037(64)90129-2.

Tegen, I. and Lacis, A. A. (1996): Modeling of particle size distribution and its influence on the radiative properties of mineral dust aerosol. *J. Geophys. Res.:Atmos.*, **101** (D14), 19237–19244, doi:10.1029/95JD03610.

Wedepohl, K. H. (1995): The composition of the continental crust. *Geochim. Cosmochim. Acta*, **59** (7), 1217–1232, doi:10.1016/0016-7037(95)00038-2.

Wientjes, I. G. M., Van de Wal, R. S. W., Reichart, G. J., Sluijs, A. and Oerlemans, J. (2011): Dust from the dark region in the western ablation zone of the Greenland ice sheet. *The Cryosphere*, **5**, 589–601, doi:10.5194/tc-5-589-2011.

Zhu, B., Yang, X., Liu, Z., Rioual, P., Li, C. and Xiong, H. (2012): Geochemical compositions of soluble salts in aeolian sands from Taklamakan and Badanjilin deserts in northern China, and their influencing factors and environmental implications. *Environ. Earth Sci.*, **66**, 337–353, doi:10.1007/s12665-011-1243-1.